7-1-2022

Topological Supercavity Resonances in the Finite System

Lujun Huang

Bin Jia

Yan Kei Chiang

Sibo Huang

Chen Shen
Rowan University, shenc@rowan.edu

See next page for additional authors

Recommended Citation

Authors

Lujun Huang, Bin Jia, Yan Kei Chiang, Sibo Huang, Chen Shen, Fu Deng, Tianzhi Yang, David A Powell, Yong Li, and Andrey E Miroshnichenko

Topological Supercavity Resonances in the Finite System

Lujun Huang,* Bin Jia, Yan Kei Chiang, Sibo Huang, Chen Shen, Fu Deng, Tianzhi Yang, David A Powell, Yong Li,* and Andrey E Miroshnichenko*

Acoustic resonant cavities play a vital role in modern acoustical systems. The ultrahigh quality-factor resonances are highly desired for some applications such as high-resolution acoustic sensors and acoustic lasers. Here, a class of supercavity resonances is theoretically proposed and experimentally demonstrated in a coupled acoustic resonator system, arising from the merged bound states in the continuum (BICs) in geometry space. Their topological origin is demonstrated by explicitly calculating their topological charges before and after BIC merging, accompanied by charges annihilation. Compared with other types of BICs, they are robust to the perturbation brought by fabrication imperfection. Moreover, it is found that such supercavity modes can be linked with the Friedrich–Wintgen BICs supported by an entire rectangular (cuboid) resonator sandwiched between two rectangular (or circular) waveguides and thus more supercavity modes are constructed. Then, these coupled resonators are fabricated and such a unique phenomenon—moving, merging, and vanishing of BICs—is experimentally confirmed by measuring their reflection spectra, which show good agreement with the numerical simulation and theoretical prediction of mode evolution. The results may find exciting applications in acoustic and photonics, such as enhanced acoustic emission, filtering, and sensing.

1. Introduction

Acoustic resonators constitute the fundamental element of many modern acoustic devices. They can be used as unit cells of acoustic metasurface that allow for arbitrary manipulation of acoustic wavefront,[1,2] leading to practical applications including acoustic absorbers[3] and invisibility cloaking.[4] The most typical example is the Helmholtz resonator, widely used in the sound absorber and for noise control. For applications such as acoustic filters, sensors, and sound lasers, acoustic resonances with ultrahigh quality-factor (*Q*-factor) are desired. Bound states in the continuum (BICs), also known as trapping mode with infinite large *Q*-factor, have triggered extensive interest in photonic and acoustic communities.[5,6] It corresponds to a nonradiating mode embedded within the continuum, enabling the enhanced light–matter interaction due to its excellent field confinement.[7–9] Different types of BICs, including symmetry-protected BICs,[10–12] Friedrich–Wintgen BICs,[13–15] Fabry–Perot

BICs,[16] and mirror-induced BICs,[17] have been reported theoretically with various acoustic systems. Also, some efforts have been made to demonstrate the existence of those BICs experimentally.[17–21] The highest reported *Q*-factor is up to 583.[17] However, most of the experimentally demonstrated BICs so far are quite sensitive to the perturbation of structure; that is, the *Q*-factor is inversely proportional to the perturbation square.[22] Thus, the following questions remain open: how to build topologically stable BICs (also called supercavity resonances or super-BICs) robust to fabrication imperfections.[23]

This work presents a synergic effort of theoretical design and experimental verification of super-BICs in a coupled acoustic resonator system arising from merged BICs. Unlike topological BICs happening in the momentum space by periodic structures, the merged BIC effect is implemented in geometry parameter space (i.e., the width of the individual resonator and the gap between them) with a two coupled resonators system. It is attributed to topological charges merging and annihilation. Also, we unveil the subtle correlation between such supercavity resonances and Friedrich–Wintgen BICs in an entire rectangular (or cuboid)-waveguide system. We fabricated such kinds of coupled resonators and experimentally verified the merging effect of BICs by measuring their reflection spectra, which show excellent agreement with the numerical calculations. Notably, the effect of

L. Huang, Y. K. Chiang, F. Deng, D. A Powell, A. E Miroshnichenko
School of Engineering and Information Technology
University of New South Wales
Northcott Drive, Canberra, ACT 2600, Australia
E-mail: lujun.huang@unsw.edu.au;
andrey.miroshnichenko@unsw.edu.au

B. Jia, S. Huang, Y. Li
Institute of Acoustics
Tongji University
Shanghai 200092, P. R. China
E-mail: yongli@tongji.edu.cn

C. Shen
Department of Mechanical Engineering
Rowan University
Glassboro, NJ 08028, USA

T. Yang
School of Mechanical Engineering and Automation
Northeastern University
Shenyang 110819, China

ADVANCED
SCIENCE NEWS
www.advancedsciencenews.com

ADVANCED SCIENCE
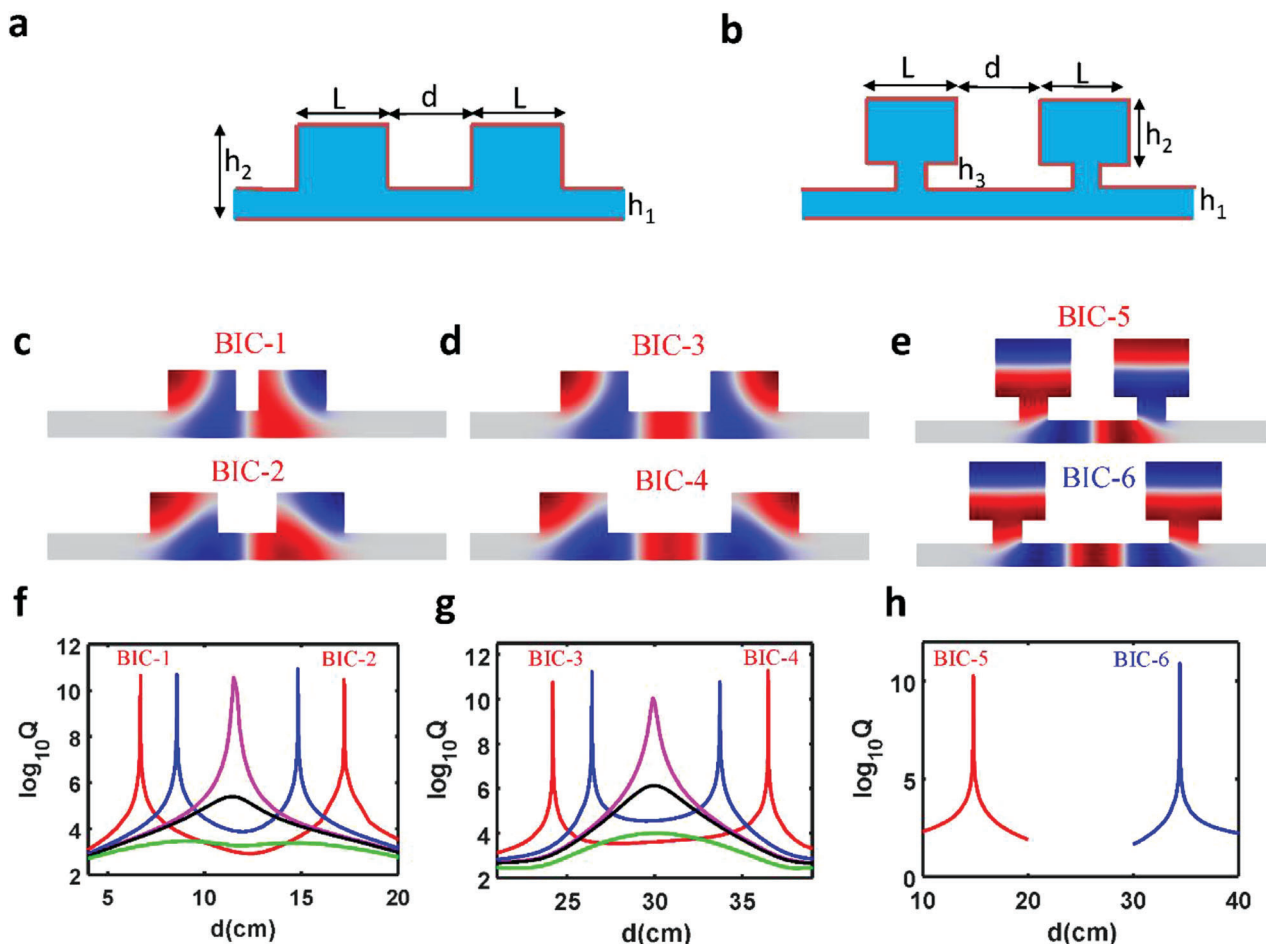Open Access
www.advancedscience.com

Figure 1. BICs in the coupled-resonator system. a) Schematic drawing of the coupled-resonator without neck. b) Schematic drawing of the coupled resonators with a neck. c) Pressure field distribution for two antibonding BICs. d) Pressure field distribution for two bonding BICs. e) Pressure field distribution for antibonding and bonding BICs for system with neck. f) Q-factor for antibonding mode as a function of distance between two resonators for width $L = 20$ cm (red), $L = 20.2$ cm (blue), $L = 20.302$ cm (magenta), $L = 20.32$ cm (black), $L = 20.5$ cm (green) while the height of single resonator and waveguide is fixed as 20 and 8 cm, respectively. g) Q-factor for bonding mode as a function of distance between two resonators for width $L = 20$ cm (red), $L = 20.2$ cm (blue), $L = 20.302$ cm (magenta), $L = 20.32$ cm (black), $L = 20.5$ cm (green). h) Q-factor for both bonding and antibonding modes as a function of the distance between two resonators. The width and height of each resonator are $L = 26$ and $h_2 = 20$ cm. The height of the waveguide is 8 cm. The neck width is 10 cm and height is 8 cm.

merged BICs is a universal phenomenon and can be extended to other systems, such as an electromagnetic wave. Our results offer promising applications in building high-performance acoustic and photonic devices, such as sensors, filters, and lasers.

2. Results and Discussion

2.1. Merged BIC in 2D Coupled Acoustic Resonators

We start by investigating the eigenmodes of the 2D coupled acoustic resonator, as schematically shown in **Figure 1**a,b. Our previous study has demonstrated that the leaky modes supported by such an open system play an essential role in governing the acoustic properties.[17] Each leaky mode can be represented by a complex eigenfrequency $\omega = \omega_0 - i\gamma$, where ω_0 and γ are respectively the resonant frequency and radiative decay rate. The radiative Q-factor can be obtained by $Q = \omega_0 / 2\gamma$. With the information of complex eigenfrequency for given modes, both reflec-

tion and transmission spectrum can be well reproduced based on temporal coupled-mode theory. Thus, the task of searching for BIC turns to find the leaky modes with zero radiative decay rate. For the sake of simplicity, we fix the waveguide and side resonator's height as $h_1 = 8$ cm and $h_2 = 20$ cm, respectively. We first consider the case of coupled resonators with the width $L = 20$ cm while the distance between two resonators is varied. Such coupled resonators support bonding mode and antibonding mode, similar to the interaction of two molecules. Figure 1c,d shows the pressure distribution of antibonding mode M_{12a} and bonding mode M_{12b}. Previous studies indicated that these two modes become BIC (called as Fabry–Perot BIC[5,16,24,25]) only when the propagating phase between two resonators satisfies $\varphi = k_0 d = m\pi$, where k_0 is the resonant wavenumber of single resonator and d is the distance between two resonators. Based on this prediction, one should be able to find one antibonding and one bonding BICs for $d \leq \lambda_0$ (λ_0 is resonant wavelength of single resonator) and the distance difference should be

**ADVANCED
SCIENCE NEWS**

www.advancedsciencenews.com

**ADVANCED
SCIENCE**
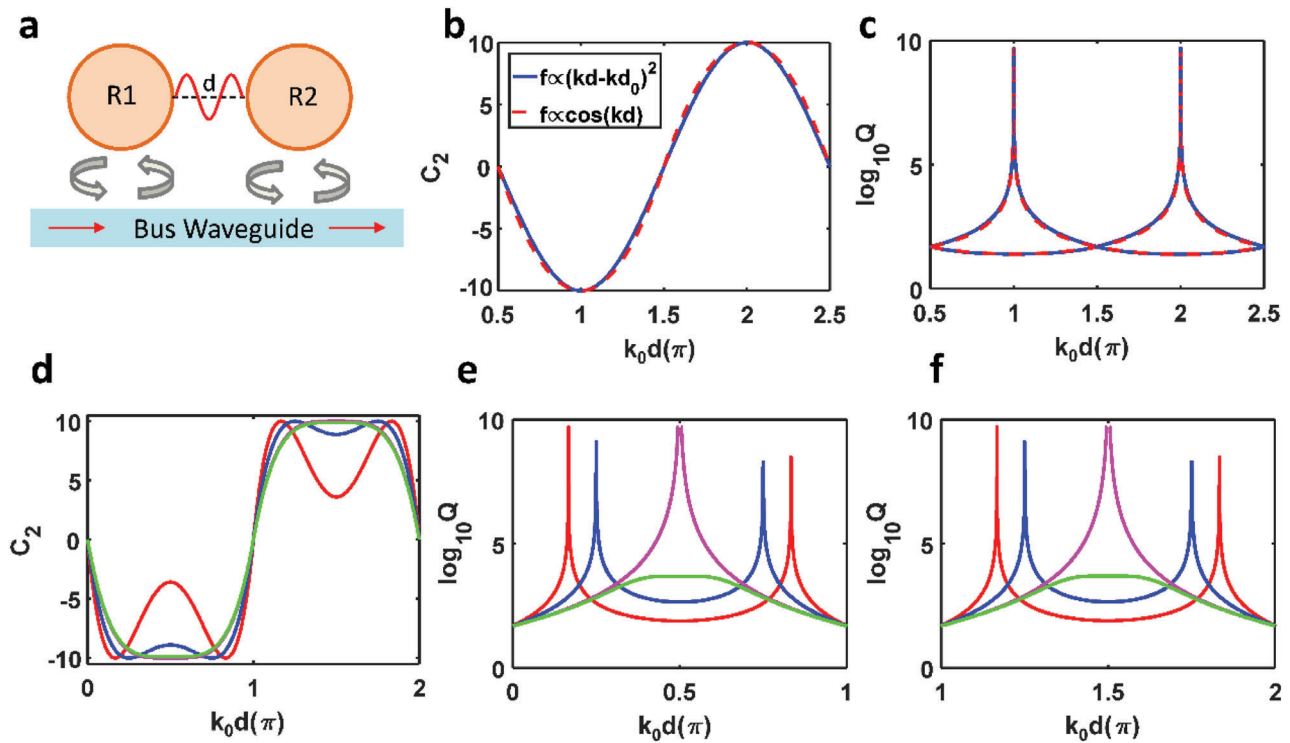Open Access

www.advancedscience.com

Figure 2. Coupled mode theory for merged BICs. a) Schematic drawing of the coupled-resonators system via a bus waveguide. b) The imaginary part of coupling C2 versus propagation phase $k_0 d$ for normal Fabry–Perot BICs. c) Q-factors of bonding and antibonding modes as a function of propagation phase $k_0 d$. d) The imaginary part of coupling C2 versus propagation phase $k_0 d$ for merged BICs cases. Note that red line represents $k_0 d_1 = \pi/6$ and $k_0 d_2 = 5\pi/6$, blue line represents $k_0 d_1 = \pi/4$ and $k_0 d_2 = 3\pi/4$, magenta line represents $k_0 d_1 = k_0 d_2 = \pi/2$, green line represents $k_0 d_1 = k_0 d_2 = \pi/2$ and A = 0.99. e,f) Q-factors of e) antibonding mode and f) bonding mode versus $k_0 d$.

close to $\lambda_0/2$. Quite surprisingly, we found from Figure 1f,g that there are two antibonding BICs and two bonding BICs. Importantly, the distance difference between two antibonding BICs (or bonding BICs) is less than $\lambda_0/2$ while the distance difference between first (second) antibonding BIC and first (second) bonding BIC is close to $\lambda_0/2$. The BICs will move toward each other if we further increase the resonators' width. When L approaches the critical value $L_c = 20.302$ cm, a merged BIC is observed. For $L > L_c$, BIC vanishes and is reduced to quasi-BIC (QBIC). Furthermore, we found that for the structure that shows BIC before merging, the Q-factor of each BIC is inverse proportional to $1/(d - d_{BIC})^2$ (see Figure S1a, Supporting Information).[22] When two antibonding (or bonding) BICs merge, the Q factor of each BIC is inverse proportional to $1/(d - d_{BIC})^4$ (see Figure S1b, Supporting Information). This phenomenon is similar to the case of merged BIC observed in the photonic system, where topological charges move toward the Γ point in first Brillouin zone at momentum space.[23,26–28] The essential difference lies in that the merging effect is observed in momentum space for an array of photonic nanoresonators, but it happens in geometry parameter space for coupled acoustic resonators.

The behavior of BICs moving, merging, and vanishing is confirmed by the reflection spectrum mapping of coupled resonators with $L = 20$, 20.302, 20.50 cm (see Figure S2, Supporting Information). This interesting phenomenon could be correlated to the strong near-field coupling of two resonators, evidenced by the rotation field distribution as shown in Figure 1c,d. To prove that strong near-field coupling indeed plays a vital role in the forma-

tion of super-BIC, we introduce a neck between the resonator and bus waveguide, as schematically drawn in Figure 1b. The Q-factor of bonding and antibonding modes versus distance are calculated and shown in Figure 1e,h. Indeed, only one antibonding BIC and one bonding BIC, belonging to normal Fabry–Perot BICs, are observed as its Q-factor is inverse proportional to $1/(d - d_{BIC})^2$ (see Figure S3a, Supporting Information). This phenomenon is also confirmed by the reflection mapping shown in Figure S3b in the Supporting Information.

Importantly, such a merging effect can be well explained by the temporal coupled-mode theory. **Figure 2**a shows the schematic drawing of such a coupled-resonators system, whose Hamiltonian takes the following general forms[29]

$$H = \begin{pmatrix} \omega_0 - i\gamma & C_1 + iC_2 \\ C_1 + iC_2 & \omega_0 - i\gamma \end{pmatrix} \tag{1}$$

where ω_0 and γ are the resonant frequency and radiative decay rate, respectively. C_1 and C_2 are the real and imaginary parts of complex coupling between two resonators. Solving Equation (1) gives us

$$\omega_+ = \omega_0 + C_1 - i\left(\gamma - C_2\right) \tag{2a}$$

$$\omega_- = \omega_0 - C_1 - i\left(\gamma + C_2\right) \tag{2b}$$

where ω_+ and ω_- are, respectively, the complex eigenfrequencies of bonding and antibonding modes. From Equation (2), we can

find that bonding (antibonding) modes become BIC for $C_2 = \pm \gamma$, while C_1 plays a minor role in the BICs' formation. Previous studies have demonstrated that such a coupled-resonator system support Fabry–Perot BICs[5] by assuming $C_1 = \kappa + \gamma \sin(k_0 d)$ and $C_2 = -\gamma \cos(k_0 d)$, where $k_0 = \omega_0 /c$ and κ is the near-field coupling term. When the phase accumulation $k_0 d = m\pi$, either bonding or antibonding mode reduces to an ideal BIC.

However, they are not the only complex coupling terms that produce the Fabry–Perot BICs. For the sake of simplicity, we assume bonding and antibonding BICs occur at $k_0 d_1 = \pi$ and $k_0 d_2 = 2\pi$. Except for $C_2 = -\gamma \cos(k_0 d)$, we found that Fabry–Perot (FP)-BICs could be successfully constructed by setting $C_2 = \gamma[-1 + A(k_0 d - \pi)^2]$ ($\pi/2 < k_0 d \leq 3\pi/2$) and $C_2 = \gamma[1 - A(k_0 d - 2\pi)^2]$ ($3\pi/2 < k_0 d \leq 5\pi/2$), where $A = 1/(1.5\pi - \pi)^2$.

Figure 2b shows C_2 as a function of the propagation phase $k_0 d$. We also plot the function $C_2 = -\gamma \cos(k_0 d)$ to make a comparison. Surprisingly, we find that these two functions almost overlap with each other. Additionally, since the real part of the coupling term shows no contribution to the formation of BICs, we assume $C_1 = 10$ Hz. Also, without losing generality, ω_0 and γ are fixed as 1000 and 10 Hz, respectively. Substituting these parameters into Equation (2) gives us the complex eigenfrequencies of bonding and antibonding modes, which are plotted in Figure 2c. Due to the similar C_2 functions, bonding (antibonding) modes have almost the same Q-factors. Note that around both BICs their Q-factors are indeed inversely proportional to $(k_0 \Delta d)^2$.

After having this knowledge, it is straightforward to construct the complex coupling term for merged BICs cases. We still assume $C_1 = 10$ Hz, $\omega_0 = 1000$ Hz, and $\gamma = 10$ Hz, while C_2 is written as follows

$$C_2(k_0 d) = \gamma[-A + B(k_0 d - k_0 d_1)^2 (k_0 d - k_0 d_2)^2] (0 < k_0 d \leq \pi) \quad (3a)$$

$$C_2(k_0 d) = \gamma[A - B(k_0 d - k_0 d_3)^2 (k_0 d - k_0 d_4)^2] (< k_0 d \leq 2\pi) \quad (3b)$$

where $A = 1$ before BIC merging and BIC merging, and $A = 1 - \delta$ after BIC merging. Here, δ is a small perturbation term that converts BIC into QBIC after BIC merging. B can be obtained based on the continuity condition at $k_0 d = \pi$. It is necessary to point out that there is an additional requirement $k_0 d_3 = k_0 d_1 + \pi$ and $k_0 d_4 = k_0 d_2 + \pi$. Figure 2d shows an example of C_2 built from Equation (3) with different $k_0 d_1$ by assuming $k_0 d_1 + k_0 d_2 = \pi$. Figure 2e,f shows the Q-factors of both antibonding and bonding modes as a function of distance. It is evident that this simple model has successfully predicted BIC moving, merging, and vanishing. Also, the Q-factors for both modes around BICs are inversely proportional to $(k_0 \Delta d)^{[2]}$ before BIC merging. When $k_0 d_1 = k_0 d_2 = \pi/2$ and $k_0 d_3 = k_0 d_4 = 3\pi/2$ two antibonding (bonding) BICs merge and their Q-factors are now inversely proportional to $(k_0 \Delta d)^{[4]}$. Note that this C_2 function is not the only one that could generate merged BICs. Another effective C_2 function could be easily constructed by replacing $(k_0 d - k_0 d_i)^2$ with $[1 - \cos(k_0 d - k_0 d_i)]$ ($i = 1, 2, 3, 4$) (see Figure S4, Supporting Information).

2.2. General Merged BICs in 2D Coupled Acoustic Resonators

Note that the case in Figure 1f,g is not the only structure that shows BIC merging effect. One could construct many merged BICs by checking the Friedrich–Wintgen BIC in an open system.[15,17,30] Here, we consider two open acoustic systems, as shown in **Figure 3**a. One is made of an acoustic cavity connecting to two waveguides with left and right open boundaries. The other corresponds to an acoustic cavity coupled to a single port waveguide. As demonstrated in our previous work, some of the BICs supported in these two systems share similar features due to the mirror-effect.[17] Taking mode M_{13} as an example, from Figure 3b,c, we indeed found that both structures support a BIC at critical size ratio $R_c \approx 0.992$ while the pressure distribution of BICs is one-quarter of the pressure distribution for the former one owning to the hard wall boundary induced mirror effect. Moreover, the eigenfield profile of BIC for the single cavity-single port waveguide system shares similar field distribution of half in coupled resonators. This suggests that one may find more merged BICs by constructing a Friedrich–Wintgen BIC with eigenfield profile that possesses symmetry along both x- and y-axes in the full cavity-waveguide system. We confirm this hypothesis by finding more examples on merged BIC in such a coupled resonators system. Here, we show one of them in Figure 3d–f, where the height of waveguide is $h_1 = 5$ cm and the height of resonator is $h_2 = 30$ cm. The red, blue, magenta, and black lines represent the case of coupled resonators with the width $L = 20, 20.4, 20.674$, and 20.7 cm, respectively. Note that only antibonding BICs are shown here to illustrate the merging effect and results of bonding BICs are given in Figure S5 in the Supporting Information. From Figure 3f, antibonding BICs indeed experience moving, merging, and vanishing with the increasing width of rectangular cavity but a fixed height. However, the left and right BICs have different moving speed toward the merged point due to the asymmetric distribution with respect to the diagonal of single resonator. More examples can be found in Figures S6 and S7 in the Supporting Information. Besides, by taking advantage of mirror effect, we found that even single resonator with mirror on the right boundary could support such a merging BICs, which has been demonstrated in Figure 3g–i. In addition, as pointed out in previous section, the common feature of such BICs is that they have rotated pressure distribution with respect to x axis, which indicates a strong near-field coupling. Thus, we can construct merged BIC in different coupled resonator system that also ensures the strong near-field coupling. The corresponding results are summarized in Figure S8 in the Supporting Information.

2.3. Topological Origin of the Merged BICs

The merging effect of two BICs in such a coupled-resonator system could be perfectly explained from a topological perspective. Unlike the case of photonic BIC, where each BIC carries a topological charge in momentum space,[26,31] we found that each BIC in such a finite acoustic system is represented by a pair of topological charges with one $q = +1$ and the other $q = -1$.[32] Without loss of generality, we consider the single-resonator-single port system shown in Figure 3g as an example and set the resonator's height and width as 20 cm. From Figure 3i, it can be seen that there are two BICs when the distance changes from 20 to 40 cm. To define the topological charge of BICs, an ultrasmall artificial loss has been introduced in the sound veloc-
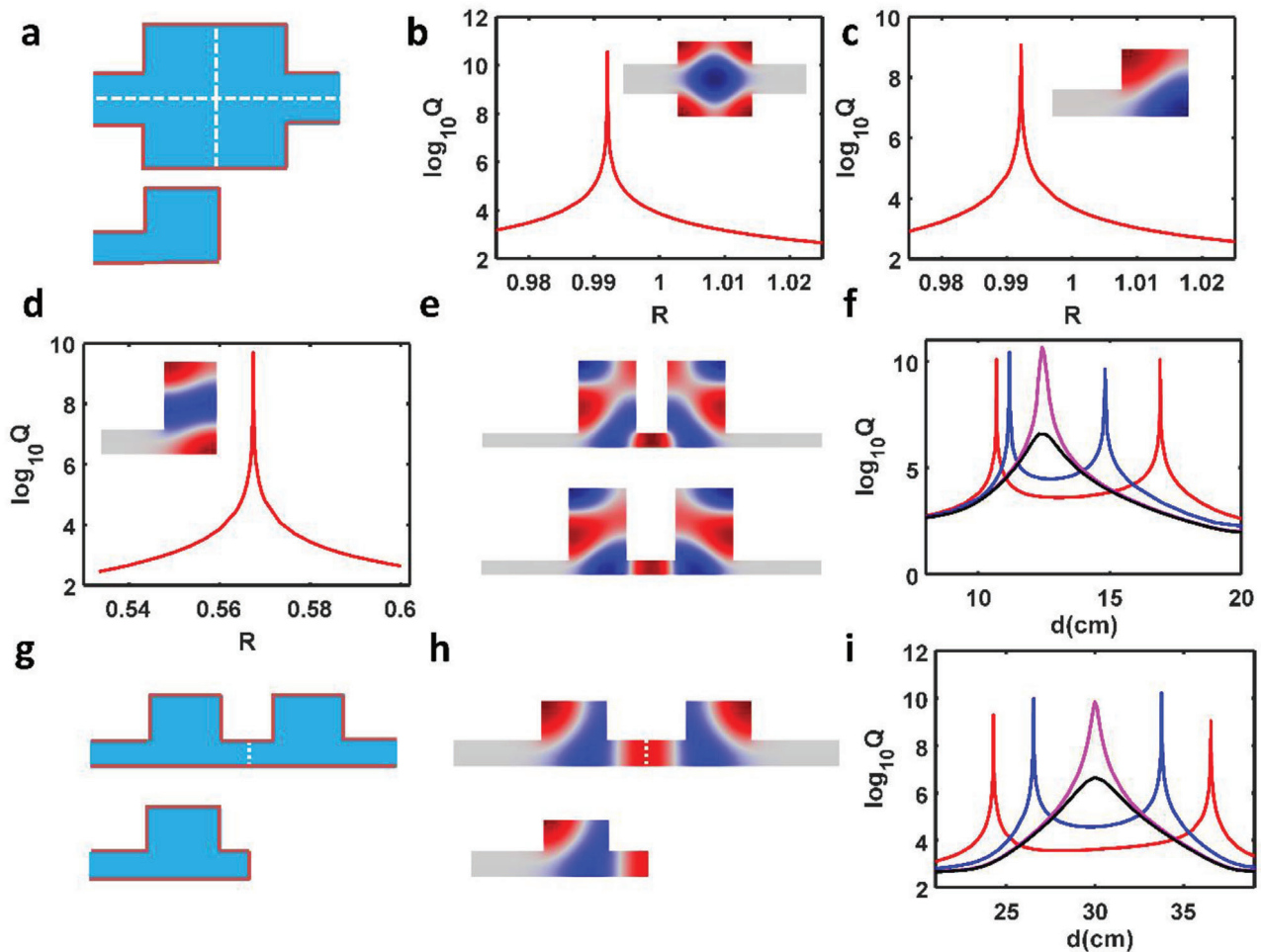
**ADVANCED
SCIENCE NEWS**

www.advancedsciencenews.com

**ADVANCED
SCIENCE**
Open Access

www.advancedscience.com

Figure 3. General features of merged BICs. a) Schematic drawing of a full-rectangular resonator sandwiched between two rectangular waveguides (top panel) and a quarter-rectangular resonator connected to single-port rectangular waveguide (bottom panel). b) Q-factor versus size ratio R ($R = Ly/Lx$) for the full-resonator system. The inset shows the pressure field distribution of Friedrich–Wintgen BIC. c) Q-factor versus size ratio R ($R = Ly/Lx$) for the quarter-resonator system. The inset shows the pressure field distribution of BIC. d) Another example of BIC supported by a quarter-resonator-single-port waveguide system. Q-factor versus size ratio R ($R = Ly/Lx$) for the quarter-resonator system. The inset shows the pressure field distribution of this BIC. e) Pressure field distribution for two antibonding BICs. f) Q-factor for antibonding mode as a function of distance between two resonators for width $L = 20$ cm (red), 20.4 cm (blue), 20.674 cm (magenta), and 20.7 cm (black). g) Schematic drawing of coupled-resonator and single resonator with mirror. h) Pressure field distribution of bonding BICs in a coupled resonators system (up) and BIC in single resonator-single port system (bottom). i) Q-factor for bonding mode as a function of distance between resonator and right boundary of system for width $L = 20$ cm (red), $L = 20.2$ cm (blue), $L = 20.301$ cm (magenta), $L = 20.31$ cm (black).

ity to quench the reflection amplitude to zero (or perfect absorption) by critical coupling. As the reflection is reduced to zero, its phase could not be clearly defined and thus could be viewed as a phase-singularity. Here, it is worth noting that there are always two phase-singularities around each BIC when a slight loss is intentionally introduced. The topological charge that each phase-singularity carries is defined as the accumulated phase when a closed path encircles the phase-singularity counter-clockwise in the distance-frequency plane

$$q = \frac{1}{2\pi} \oint d\varphi \qquad (4)$$

Indeed, there are two zero-reflection points in amplitude mapping, as shown in **Figure 4**a,b. Each zero-reflection point corre-

sponds to a phase vortex in the phase mapping of Figure 4e,f. Then, we calculate the phase along a closed path encircling the phase-vortex indicated by a yellow rectangle in Figure 4a,b and plot it in Figure S9 in the Supporting Information. By using Equation (4), the topological charges can be evaluated to $q_1 = +1$ and $q_2 = -1$ for the two-phase vortices, respectively. Similarly, the second BIC carries topological charge pair $q_3 = +1$ and $q_4 = -1$. Thus, we can conclude that each BIC could be correlated to a pair of opposite topological charges. When the width of the resonator increases to 20.301 cm, these two BICs merge and are reduced to a single BIC, as confirmed by Figure 4c,g. Also, topological charge analysis indicates that the middle two topological charges coalesce and exhibit and only one pair of topological charges is left (see Figure S10, Supporting Information), indicating the merging BICs. Further increasing the resonator's width
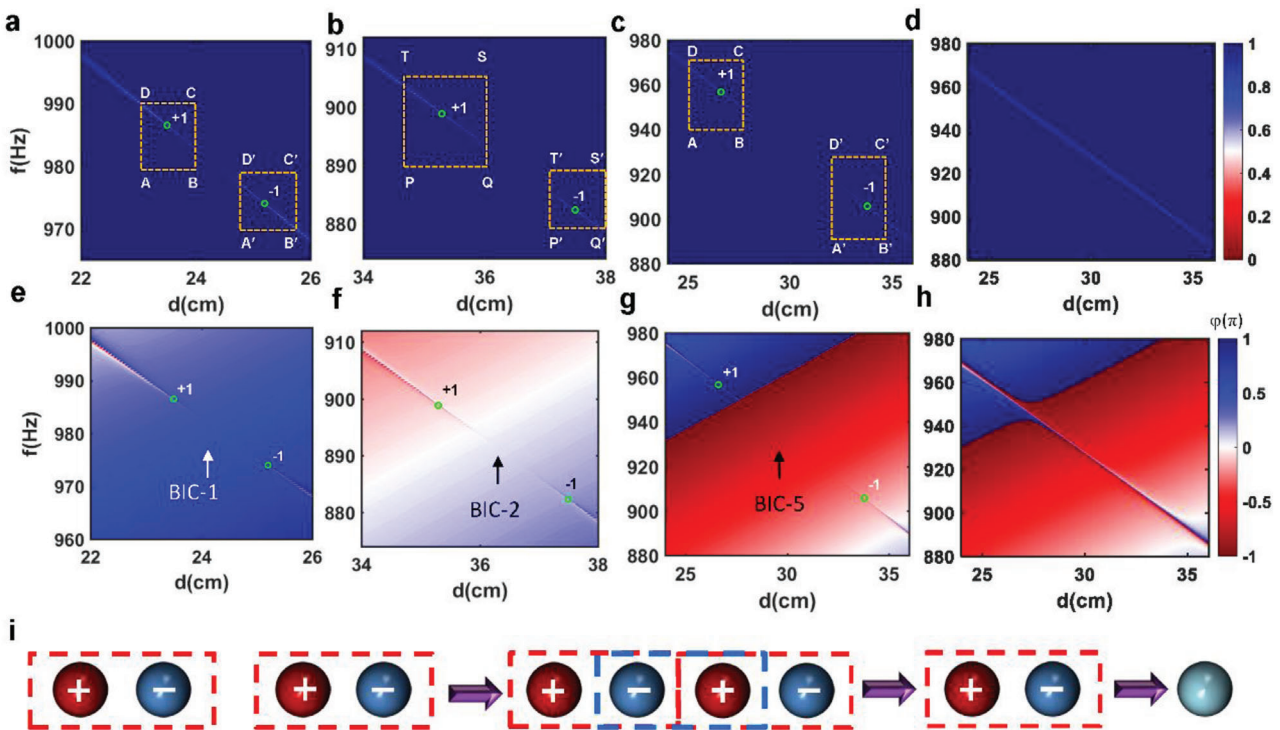
Figure 4. Topological explanation of merged BICs. a,b) Reflection mapping of the single resonator with a mirror around a) BIC-1 and b) BIC-2 before merging. An artificial loss is introduced in the sound velocity ($v = 343*(1 + 2.5 \times 10^{-5}i)$). c) Reflection mapping for merged BIC. d) Reflection mapping after BIC merging. e,f) Phase mapping of the single resonator with a mirror around e) BIC-1 and f) BIC-2. g) Phase mapping for merged BIC. h) Phase mapping after BIC merging. i) Topological charge evolution process before and after BIC merging.

leads to the vanishing of BIC. No topological charge will be found for this structure because the critical coupling is no longer satisfied, as verified in Figure 4d,h. Figure 4i summarizes the entire process of BIC moving, merging, and vanishing by computing the topological charge evolution. Two pairs of topological charges move to each other, annihilate, and disappear finally.

2.4. Experimental Demonstration of the Merged BIC in 3D Coupled-Resonators

Such merged BICs also happen in 3D cases, where two cuboid resonators coupled with each other via an acoustic waveguide (e.g., a circular waveguide or a rectangular waveguide), as schematically shown in **Figure 5**a. Here, the diameter of the waveguide is 29 mm for the sake of experimental consideration. The length and height of the cuboid resonator are fixed as 29 and 60 mm, respectively. By varying the length of the cuboid resonator from $L = 60$, 61, 62.212, to 63 mm, from Figure 5a–c, we indeed observe the similar effects of BICs moving, merging, and vanishing when the distance between coupled resonators is continuously changed. Similar to 2D cases, we can find more merged BICs by constructing Friedrich–Wintgen BICs, as shown in Figures S11–S13 in the Supporting Information. To experimentally verify the merging BIC, we fabricate a series of coupled resonators-waveguide structures. Figure 5d shows the optical images of two printed samples. The lengths of each resonator are chosen as $L = 61$, 62.2, 63 mm, while the distance between resonators covers a broad range from 10 to 140 mm. Figure 5e–g

shows the measured reflection mapping, while Figure 5h–j displays the calculated reflection spectrum. Excellent agreement is found between the experiments and simulations. For $L = 61$ mm, there are two antibonding BICs and two bonding BICs. When L is increased to 62.2 mm, both bonding BICs and antibonding BICs start merging. Further increasing L leads to the vanishing of BIC.

2.5. Generalization of Merged BIC to Photonic Waveguide System

Finally, it is worth commenting that such merged BICs are not limited to the acoustic wave. It could also be generalized to other systems supporting wave-like excitations, such as electromagnetic structures. To construct merged BICs, one just needs to replace the rigid wall boundary of a coupled acoustic resonator system with either perfect electric conductor or perfect magnetic conductor, depending on the polarization choice. The examples are shown in Figure S14 in the Supporting Information for transverse electric polarization and Figure S15 in the Supporting Information for transverse magnetic polarization in the supplementary materials. Thus, we can envision many exciting applications that could be developed based on such a coupled photonic resonator system, such as a high-performance filter at the microwave range.

3. Conclusion

We proposed the theoretical design and experimental demonstration of supercavity resonances in two coupled acoustic resonators
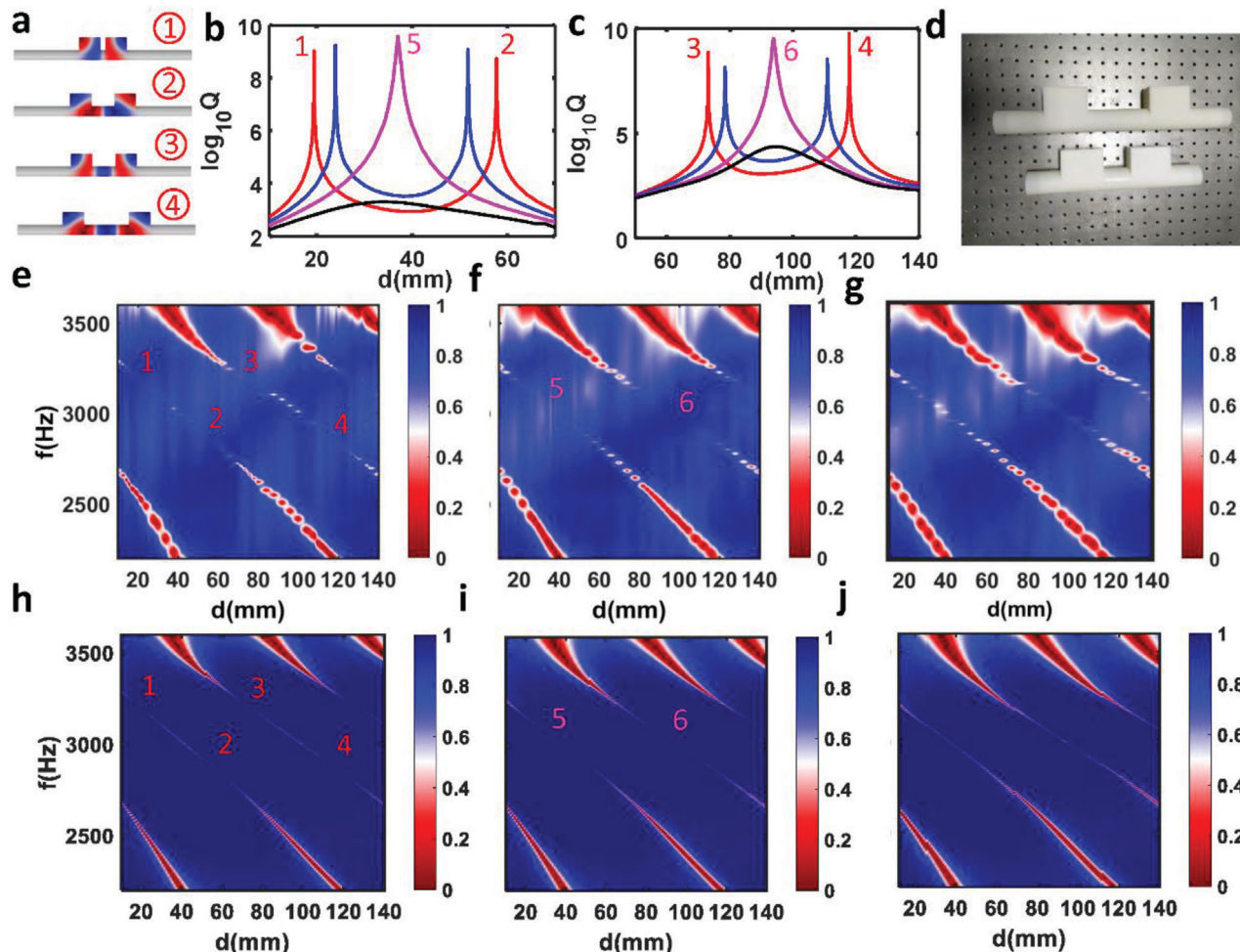
Figure 5. Experimental demonstration of merged BICs in 3D coupled resonator system. a) Pressure field distribution for two antibonding BICs (#1–2) and two antibonding BICs (#3–4). b) Q-factor for antibonding mode as a function of distance between two resonators for width $L = 61$ mm (red), 61.6 mm (blue), 62.212 mm (magenta), and 63 mm (black). The diameter of circular waveguide is 29 mm. c) Q-factor for bonding mode as a function of distance between two resonators for width $L = 61$ mm (red), 61.6 mm (blue), 62.212 mm (magenta), 63 mm (black). d) Optical image of 3D coupled resonator system fabricated by 3D-printing. e–g) Measured reflection spectrum mapping versus distance between two resonators for the resonator's width e) $L = 61$ mm, f) $L = 62.2$ mm, and g) $L = 63$ mm. h–j) Simulated reflection spectrum mapping versus distance between two resonators for the resonator's width h) $L = 61$ mm, i) $L = 62.2$ mm, and j) $L = 63$ mm.

arising from merged BICs. Their formation could be perfectly explained by their topological charges' evolution. Additionally, we found that strong near-field coupling plays an essential role in constructing such merged BICs. We also unveiled the general rules of finding out such kinds of supercavity resonances, which could be rigorously correlated to the Friedrich–Wintgen BIC in an entire rectangular resonator with two ports connecting to waveguide. Following this rule, we could construct two equivalent systems which are also able to support supercavity resonances. Moreover, we demonstrate that the topological characteristics of the merging effect are explained by the topological charges carried by the reflection phase singularity. Finally, we fabricated a series of samples and demonstrated their peculiar property in two coupled 3D resonators-BICs moving, merging, and vanishing. Our results may find applications in constructing high-performance acoustic devices, such as acoustic filters, acoustic sensors, acoustic lasers, etc.

4. Experimental Section

Simulation: Both the eigenmodes and reflection/transmission spectra are performed with the commercial software COMSOL Multiphysics. The speed of sound and air density is set as 343 m s^{-1} and 1.29 kg m^{-3}, respectively. When calculating eigenmodes and reflection spectrum, perfect matched layer boundaries at the two ends of waveguides are applied to mimic acoustic wave propagation in the infinite space. The other exterior boundaries are set as hard walls.

Experiment: These coupled acoustic resonators are fabricated with 3D-printing technology using laser sintering stereolithography (140 μm) with a photosensitive resin (UV curable resin). Reflection spectra of these samples are measured using a Brüel and Kjær type-4206T impedance tube with a diameter of 29 mm. A loudspeaker generates a plane wave and the amplitude and phase of local pressure are measured by four 1/4-in. condenser microphones (Brüel and Kjær type-4187) situated at designated positions.

Statistical Analysis: All experiments were performed at least twice to confirm the reproducibility of the results. All of simulated and measured

**ADVANCED
SCIENCE NEWS**

www.advancedsciencenews.com

**ADVANCED
SCIENCE**
Open Access

www.advancedscience.com

data are directly collected and presented without preprocessing and post-processing.

Supporting Information

Supporting Information is available from the Wiley Online Library or from the author.

Conflict of Interest

The authors declare no conflict of interest.

Data Availability Statement

The data that support the findings of this study are available from the corresponding author upon reasonable request.

[1] B. Assouar, B. Liang, Y. Wu, Y. Li, J.-C. Cheng, Y. Jing, *Nat. Rev. Mater.* **2018**, *3*, 460.
[2] Y. Li, X. Jiang, R.-Q. Li, B. Liang, X.-Y. Zou, L.-L. Yin, J.-C. Cheng, *Phys. Rev. Appl.* **2014**, *2*, 64002.
[3] Y. Li, B. M. Assouar, *Appl. Phys. Lett.* **2016**, *108*, 063502.
[4] S. Zhang, C. Xia, N. Fang, *Phys. Rev. Lett.* **2011**, *106*, 24301.
[5] C. W. Hsu, B. Zhen, A. D. Stone, J. D. Joannopoulos, M. Soljačić, *Nat. Rev. Mater.* **2016**, *1*, 16048.
[6] A. F. Sadreev, *Rep. Prog. Phys.* **2021**, *84*, 055901.
[7] A. Kodigala, T. Lepetit, Q. Gu, B. Bahari, Y. Fainman, B. Kanté, *Nature* **2017**, *541*, 196.
[8] L. Xu, K. Zangeneh Kamali, L. Huang, M. Rahmani, A. Smirnov, R. Camacho-Morales, Y. Ma, G. Zhang, M. Woolley, D. Neshev, A. E. Miroshnichenko, *Adv. Sci.* **2019**, *6*, 1802119.
[9] K. Koshelev, S. Kruk, E. Melik-Gaykazyan, J.-H. Choi, A. Bogdanov, H.-G. Park, Y. Kivshar, *Science* **2020**, *367*, 288 LP.
[10] S. Hein, W. Koch, *J. Fluid Mech.* **2008**, *605*, 401.
[11] D. Evans, *Q. J. Mech. Appl. Math.* **1998**, *51*, 263.
[12] C. M. Linton, M. Mciver, P. Mciver, K. Ratcliffe, J. Zhang, *Wave Motion* **2002**, *36*, 67.
[13] A. A. Lyapina, D. N. Maksimov, A. S. Pilipchuk, A. F. Sadreev, *J. Fluid Mech.* **2015**, *780*, 370.
[14] A. A. Lyapina, A. S. Pilipchuk, A. F. Sadreev, *J. Sound Vib.* **2018**, *421*, 48.
[15] H. Friedrich, D. Wintgen, *Phys. Rev. A* **1985**, *32*, 3231.
[16] S. Hein, W. Koch, L. Nannen, *J. Fluid Mech.* **2012**, *692*, 257.
[17] L. Huang, Y. K. Chiang, S. Huang, C. Shen, F.u Deng, Y.i Cheng, B. Jia, Y. Li, D. A. Powell, A. E. Miroshnichenko, *Nat. Commun.* **2021**, *12*, 4819.
[18] R. Parker, *J. Sound Vib.* **1966**, *4*, 62.
[19] N. A. Cumpsty, D. S. Whitehead, *J. Sound Vib.* **1971**, *18*, 353.
[20] S. Huang, T. Liu, Z. Zhou, X.u Wang, J. Zhu, Y. Li, *Phys. Rev. Appl.* **2020**, *14*, 21001.
[21] P. J. Cobelli, V. Pagneux, A. Maurel, P. Petitjeans, *Europhys. Lett.* **2009**, *88*, 20006.
[22] K. Koshelev, S. Lepeshov, M. Liu, A. Bogdanov, Y. Kivshar, *Phys. Rev. Lett.* **2018**, *121*, 193903.
[23] J. Jin, X. Yin, L. Ni, M. Soljačić, B. Zhen, C. Peng, *Nature* **2019**, *574*, 501.
[24] I. Rotter, A. F. Sadreev, *Phys. Rev. E* **2005**, *71*, 46204.
[25] G. Ordonez, K. Na, S. Kim, *Phys. Rev. A* **2006**, *73*, 22113.
[26] B. Zhen, C. W. Hsu, L. Lu, A. D. Stone, M. Soljačić, *Phys. Rev. Lett.* **2014**, *113*, 257401.
[27] E. N. Bulgakov, D. N. Maksimov, *Phys. Rev. A* **2017**, *96*, 63833.
[28] L. Yuan, Y. Y. Lu, *Phys. Rev. A* **2017**, *95*, 23834.
[29] W. Suh, Z. Wang, S. Fan, *IEEE J. Quantum Electron.* **2004**, *40*, 1511.
[30] L. Huang, L. Xu, M. Rahmani, D. Neshev, A. E. Miroshnichenko, *Adv. Photonics* **2021**, *3*, 016004.
[31] H. M. Doeleman, F. Monticone, W. Den Hollander, A. Alù, A. F. Koenderink, *Nat. Photonics* **2018**, *12*, 397.
[32] Z. Sakotic, A. Krasnok, A. Alú, N. Jankovic, *Photonics Res.* **2021**, *9*, 1310.